Cationic Iridium (III) Complexes Bearing Ancillary 2,5-dipyridyl(pyrazine) (2,5-dpp) and 2,2':5',2''-terpyridine (2,5-tpy) ligands: Synthesis, Optoelectronic Characterization and Light-Emitting Electrochemical Cells.

Kamrul Hasan,[a] Loïc Donato,[a,b] Yulong Shen,[c] Jason Slinker[c] and Eli Zysman-Colman[d]**

[a] *Département de Chimie, Université de Sherbrooke, 2500 Boul. de l'Université, Sherbrooke, QC, Canada, J1K 2R1*
[b] *Present address: Institut de Science et Ingenierie Supramoleculaires (ISIS - UMR 7006) Universite de Strasbourg, CNRS, 8 Rue Gaspard Monge, 67000 Strasbourg (France).*
[c] Department of Physics, The University of Texas at Dallas, 800 W. Campbell Rd., Richardson, TX, 75080, USA
[d] EaStCHEM School of Chemistry, University of St Andrews, St Andrews, Fife, UK, KY16 9ST, Fax: +44-1334 463808; Tel: +44-1334 463826; E-mail: ezc@st-andrews.ac.uk; URL: http://www.zysman-colman.com

Abstract.

Four cationic iridium(III) complexes of the form $[Ir(C^N)_2(N^N)]^+$ bearing either a 2,5-dipyridylpyrazine (2,5-dpp) or a 2,2':5',2''-terpyridine (2,5-tpy) ancillary ligand and either 2-phenylpyridine (ppy) or a 2-(2,4-difluorophenyl)-5-methylpyridine (dFMeppy) cyclometalating

ligands were synthesized. The optoelectronic properties of all complexes have been fully characterized by UV-visible absorption, cyclic voltammetry and emission spectroscopy. The conclusions drawn from these studies have been corroborated by DFT and TDDFT calculations. The four complexes were assessed as emitters in light-emitting electrochemical cells. Complex **1a**, $[Ir(ppy)_2(2,5\text{-dpp})]PF_6$, was found to be a deep red emitter (666 nm) both in acetonitrile solution and in the electroluminescent device. Complex **2a**, $[Ir(ppy)_2(2,5\text{-tpy})]PF_6$ was found to be an orange emitter (604 nm) both in solution and in the LEEC. LEECs incorporating both of these complexes were stable over the course of around 4-6 hours. Complex **1b**, $[Ir(dFMeppy)_2(2,5\text{-dpp})]PF_6$, was also determined to emit in the orange (605 nm) but with a photoluminescent quantum yield (Φ_{PL}) double that of **2a**. Complex **2b**, $[Ir(dFMeppy)_2(2,5\text{-tpy})]PF_6$ is an extremely bright green emitter (544 nm, 93%). All four complexes exhibited quasireversible electrochemistry and all four complexes phosphoresce from a mixed charge-transfer excited state.

Introduction.

Light Emitting Electrochemical cells (LEECs) are a promising type of solid-state lighting device.[1] The first operational LEEC was reported by Pei *et al.* and consisted of a mixture of conjugated luminescent materials and a conductive polymer in an ionic environment.[2] Following this seminal contribution a second class of emissive materials, phosphorescent ionic transition metal complexes (iTMCs), was explored in an effort to simplify the design.[3] The main advantages of LEECs as solid-state lighting devices are: (i) simple device architectures; (ii) operation that is insensitive to the work function electrodes resulting in the use of air stable electrodes such as Al, Au and Ag and removing the requirement for encapsulation; and (iii)

facile and inexpensive processability through spin coating from polar, benign solvents such as acetonitrile (ACN) permitting access to large area lighting panels. Broadly, the mode of operation in a LEEC relies on the redistribution of mobile ions within the emissive layer upon the application of an external voltage. This redistribution generates an interfacial electrical double layer at each contact, resulting in a thinner charge injection barrier in the device.[4] Holes and electrons migrate within the emissive layer through a hopping mechanism and recombine to form an exciton, which radiatively decays producing light.

Of the large number of iTMCs incorporated into LEECs to date the best performing are cationic heteroleptic iridium(III) complexes of the form $[(C\hat{}N)_2Ir(N\hat{}N)]^+$. This observation is unsurprising given the generally high photoluminescent quantum yields (Φ_{PL}), the relatively short emission lifetimes (τ_e) for these phosphors and the ease with which this class of complexes can be color tuned.[5] Though there is a plethora of example of cationic iridium complexes emitting in the blue-green, the yellow and the orange in acetonitrile solution, there are many fewer reports of examples of green (λ_{max} near 530 nm)[6] or deep red emission (λ_{max} > 640 nm).[7]

Recently, as part of a study concerning dinuclear iridium complexes our group reported a deep red emissive Ir(III) complex $[(ppy)_2Ir(2,5\text{-dpp})]PF_6$, **1a**, where 2,5-dpp is 2,5-dipyridylpyrazine and ppyH is 2-phenylpyridine, which we assessed as a promising candidate for a red-emitting LEEC.[8] This initial result prompted us to explore the structure-property relationship between the use of 2,5-dpp versus 2,2':5',2''-terpyridine (2,5-tpy) as ancillary ligands in cationic iridium complexes both in solution and as emitters in LEECs. Herein, we report the synthesis, optoelectronic characterization and their evaluation in LEECs of four iTMCs emitting between

the deep red to green: $[(ppy)_2Ir(2,5\text{-}dpp)]PF_6$ **1a**, $[(dFMeppy)_2Ir(2,5\text{-}dpp)]PF_6$ **1b**, $[(ppy)_2Ir(2,5\text{-}tpy)]PF_6$ **2a**, $[(dFMeppy)_2Ir(2,5\text{-}tpy)]PF_6$ **2b** (dFMeppy = 2-(2,4-difluorophenyl)-5-methylpyridine). Although the preparation and UV-Vis spectroscopic characterization of **2a** had been previously been reported[9], a detailed assessment of its optoelectronic properties was absent.

Results and Discussion.

Synthesis. The targeted ancillary ligands 2,5-dpp and 2,5-tpy were obtained in moderate yield from a double Negishi coupling of 2-bromopyridine with 2,5-dibromopyrazine and 2,5-dibromopyridine, respectively (Scheme **1**). Heteroleptic cationic complexes **1a-2b** were obtained in moderate-to-good yield through cleavage of the corresponding iridium dimer, $[(C\text{^}N)_2Ir(Cl)]_2$ with each of these two N^N ligands followed by anion metathesis with $(NH_4PF_6)_{aq}$. Each complex was purified by flash chromatography. Notably, the yields of **1a-1b** were relatively lower (48-35 %) compared to those for **2a-2b** (80-85%) due to the potential of the latter to form dinuclear iridium complexes through the bridging 2,5-dpp ligand.[10] The structural identity and purity of each of the complexes were ascertained through ^1H NMR, ^{19}F NMR and ^{13}C NMR spectroscopy, ESI-HRMS and melting point analyses.

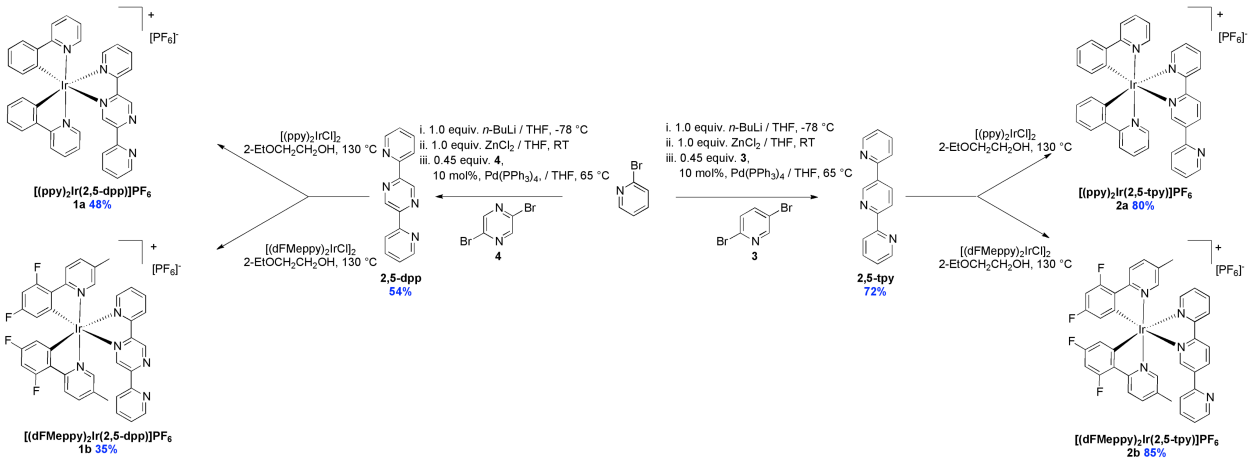

Scheme **1**. Synthesis of 2,5-dpp and 2,5-tpy N^N ligands and their corresponding iridium complexes **1a-2b**.

Cyclic voltammetry. The electrochemical behavior of **1a-2b** was investigated by cyclic voltammetry (CV) in deaerated ACN solution containing nNBu$_4$PF$_6$ as the supporting electrolyte and using Fc/Fc$^+$ as an internal standard at 298 K. All potentials are referenced to SCE (Fc/Fc$^+$ = 0.38 V in ACN).[11] The electrochemistry data are summarized in Table **1**. The CV behavior was reproducible at the faster scan rate of 200 mV·s^{-1}. The CV traces for **1a-2b** are shown in Figure **1**.

Table **1**. Electrochemical data for complexes **1a-2b**.[a]

Complex	C^N ligand	N^N ligand	$E_{pa,ox}$[b] V	$E_{1/2,red}^1$ V	ΔE_p^1 mV	$E_{1/2,red}^2$ V	ΔE_p^2 mV	ΔE V
1a	ppy	2,5-dpp	1.41	-0.98	66	-1.63	71	2.42
1b	dFMeppy	2,5-dpp	1.67	-0.94	69	-1.60	92	2.65
2a	ppy	2,5-tpy	1.33	-1.26	62	-1.79	66	2.62
2b	dFMeppy	2,5-tpy	1.59	-1.22	63	-1.75	65	2.85

[a] CV traces recorded in ACN solution with 0.1 M (n-Bu$_4$N)PF$_6$ at 298 K at 50 mV·s^{-1}. [b] Values are in V vs. SCE (Fc/Fc$^+$ vs. SCE = 0.38 V).[11] $\Delta E = \Delta E_{redox}$; $\Delta E_p = |E_{pa} - E_{pc}|$, where E_{pa} = anodic peak potential and E_{pc} = cathodic peak potential; $E_{1/2} = (E_{pa} + E_{pc})/2$ and result from one-electron processes. A non-aqueous Ag/Ag$^+$ electrode (silver wire in a solution of 0.1 M

$AgNO_3$ in ACN) was used as the pseudoreference electrode; a glassy-carbon electrode was used for the working electrode and a Pt electrode was used as the counter electrode. [b] Irreversible and E_{pa} reported for oxidation peak potentials.

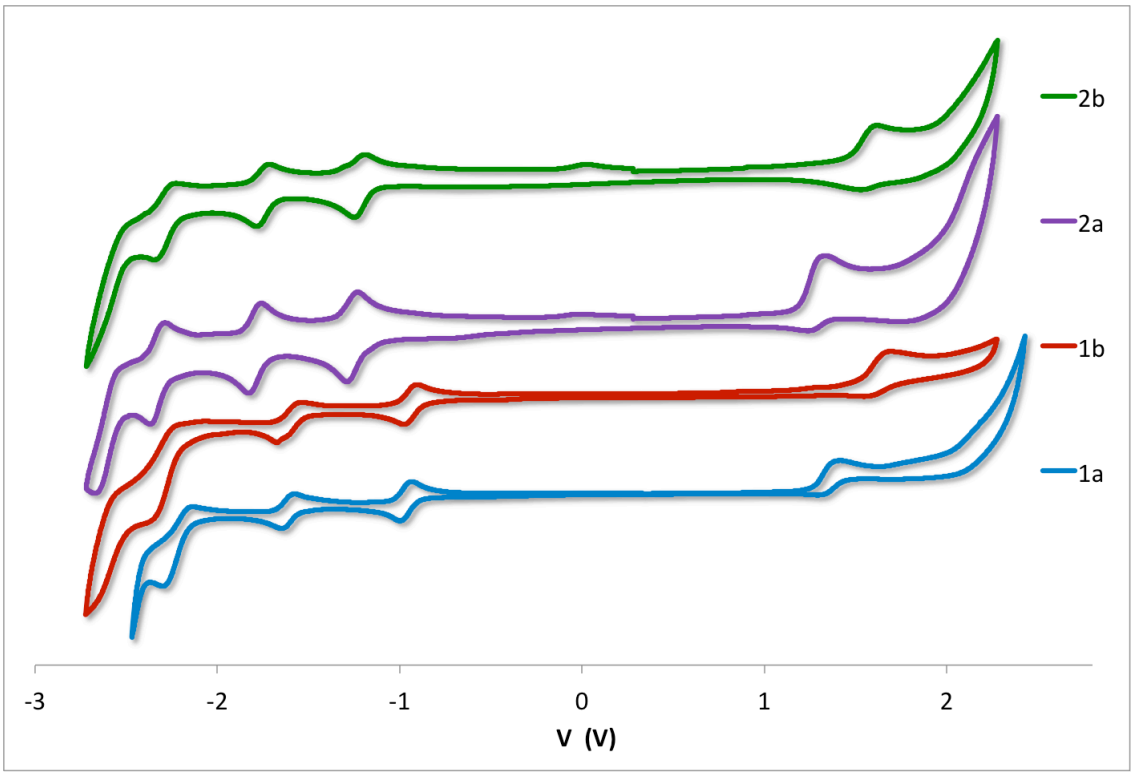

Figure **1**. CVs for **1a-2b** recorded at 298 K at 50 $mV{\cdot}s^{-1}$ in deaerated ACN with 0.1 M $(n\text{Bu}_4\text{N})PF_6$.

All complexes exhibit irreversible first oxidation waves and quasi-reversible-to-reversible reduction waves. During the anodic scan of all four complexes showed irreversible oxidation waves in between 1.33 to 1.67 V versus SCE. This oxidation waves are assigned for the redox couple of Ir^{III}/Ir^{IV} with significant contribution from the C^N ligands. These oxidation potentials are more anodically shifted compared to $[(ppy)_2Ir(bpy)]PF_6$ ($E_{1/2,ox}$ = 1.25 V) and $[(dFMeppy)_2Ir(bpy)]PF_6$ ($E_{1/2,ox}$ = 1.55 V) due to the electron withdrawing nature of 2,5-dpp and 2,5-tpy ligand.[12] The presence of the extra nitrogen in the central pyrazine ring results in a 80 mV shift to further positive potential for **1a** compared to **2a** and **1b** compared to **2b**. These trends in

anodic displacement of the oxidation wave mirror those observed with Ru. For example, the first oxidation for $[(bpy)_2Ru(2,5\text{-}dpp)](PF_6)_2$ is found at 1.67 V *vs* SCE whereas in $[Ru(bpy)_3](PF_6)_2$ it is 1.32 V.[13] It can be inferred that a similar trend exists for 2,5-tpy as the oxidation for $[(bpy)_2Ru(2,5\text{-}tpy)](PF_6)_2$ was reported to be 0.83 V *vs* Fc/Fc^+ in DMF.[14] Unsurprisingly, the oxidation waves for **1b** and **2b** are significantly anodically shifted by 260 mV compared to **1a** and **2a**, respectively because of the presence of the electron withdrawing fluoride substituents.

Upon cathodic scan, all four complexes showed three quasi-reversible reduction waves. The first two reduction processes for **1a** and **1b** are clustered found -0.94 and -0.98 and -1.60 and -1.63 V, respective. Thus, the nature of the C^N ligand has little effect on the reduction potential. These events are assigned to successive one-electron reductions of the bridging 2,5-dpp ligand based on DFT calculations and similar electrochemical behavior to $[Ru(bpy)_2(2,5\text{-}dpp)](PF_6)_2$.[15] The first reduction potentials for **1a-1b** are significantly anodically shifted compared to $[(ppy)_2Ir(bpy)](PF_6)_2$ (-1.38 V) owing to the increased conjugation and electron withdrawing character of the substituents on the N^N ligand. The first two reduction waves for **2a** and **2b** are found between -1.22 to -1.26 and -1.75 to -1.79 V, respectively. These reductions, which are shifted to positive potentials compared to $[(dFMeppy)_2Ir(bpy)](PF_6)_2$ (-1.34 V),[12] have been analogously assigned to the successive one-electron reduction processes occurring on 2,5-tpy ligand. The reduction wave in **2a** is significantly anodically shifted compared to that found for $[Ir(ppy)_2(tpy)]PF_6$ at -1.44 V, demonstrating the large impact the regiochemistry of the pyridyl substitution has on the electrochemical properties of the complex (tpy = 2,2':6',2''-Terpyridine).[7m] Notably, the impact on the reduction potentials is attenuated for **2a-2b** compared to **1a-1b**. The first two reduction waves for **2a** and **2b** are cathodically shifted by 280 and 160

mV, respectively, compared to those for **1a** and **1b**. In all cases a third reduction process is observed at more negative potential between -2.25 to -2.31 V, which is assigned to reduction of one of the C^N ligands.

UV-Visible absorption spectroscopy. The UV-visible absorption spectra for **1a-2b** were recorded in aerated ACN at 298 K and are shown in Figure **2**. The calculated molar absorptivities, ε, are reported in Table **2**. As with many cationic heteroleptic iridium complexes of the form $[(C^N)_2Ir(N^N)]^+$ the absorption spectra exhibit several characteristic features. Of note, the absorption spectrum of **2a** resembles that reported by Vos and co-workers.[9] The high energy and high intensity bands around 250 nm are assigned to the spin-allowed ligand centered (^{1}LC) π-π* transitions occurring on both sets of ligands. Indeed, These bands are slightly blue shifted in the case of dFMeppy containing complexes **1b** and **2b** while they are more intense with 2,5-dpp containing complexes **1a** and **1b**. Lower intensity absorption bands between 290-340 nm are assigned by TDDFT (see below) to admixtures of spin-allowed mixed charge transfer (^{1}CT) bands. These bands are red shifted for **1a** and **1b**, pointing to the involvement of the N^N ligand in the transition. The very low intensity absorption bands past 450 nm are assigned to mainly spin-forbidden mixed ^{3}CT bands.

The molar absorptivities for each of the absorption bands are on the order of 10^4 M^{-1} cm^{-1}. The profile and intensity of these bands are similar to other bis(heteroleptic) cationic iridium complexes reported elsewhere in the literature.[8,16]

Table **2**. Relevant spectroscopic data for complex **1a-2b**.

Complex	λ_{abs} / nm (ε /10^4 M^{-1} cm^{-1})[a]	$E_{0,0}$ (nm)
1a	252 (6.37), 290 (4.42), 334 (4.11), 375 (1.30), 460 (0.128)	663
1b	249 (7.23), 299 (4.10), 341 (3.66), 450 (0.166)	571
2a	256 (5.10), 290 (4.03), 318 (3.52), 387 (0.63), 472 (0.086)	691
2b	249 (5.24), 266 (4.73), 316 (3.53), 380 (0.39), 427 (0.067)	479

[a] Absorption spectra recorded in aerated ACN at 298 K. Molar absorptivities (ε) determined over a concentration range of 1.02 x 10^{-5} to 1.33 x 10^{-5} M. [b] $E_{0,0}$ was estimated from the onset of the absorption spectrum at approximately 10% intensity.

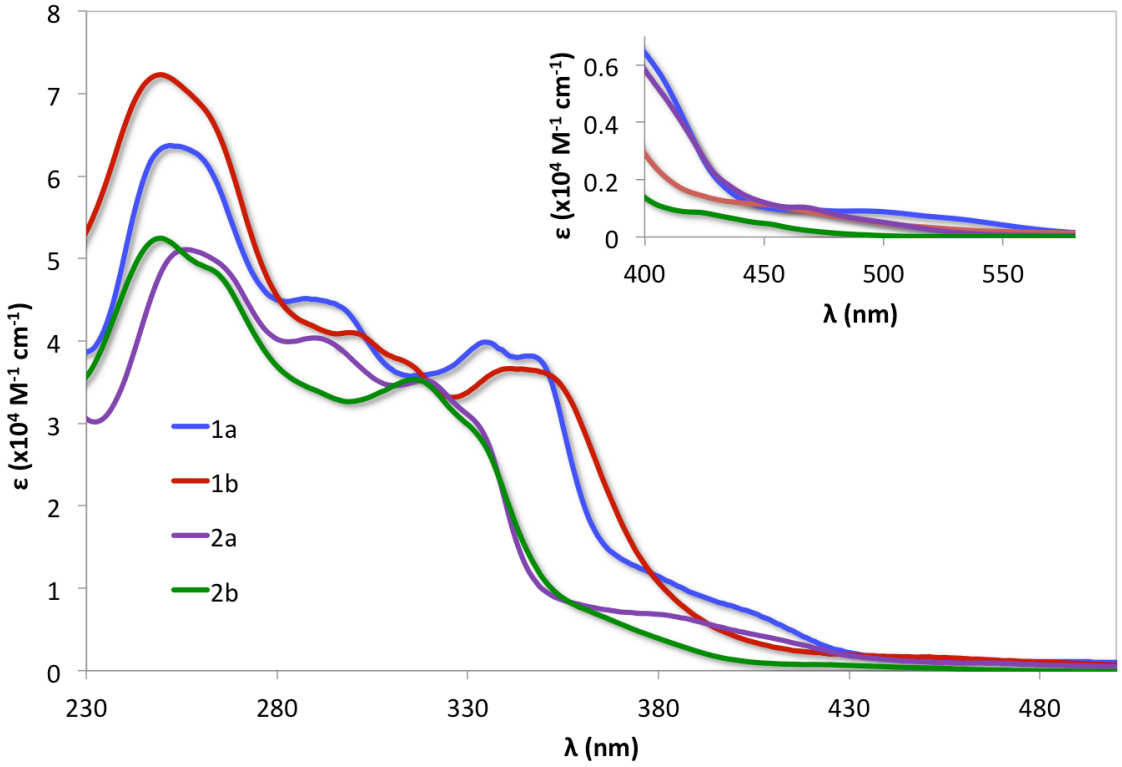

Figure **2**. UV-visible absorption spectra for **1a-2b** in ACN at 298 K. Inset: Zoomed UV-visible spectra for the region between 400-600 nm.

Solution state photophysical behavior. The steady state emission spectra for complexes **1a-2b** were recorded in degassed ACN at 298 K and are shown in Figure **3** with the associated photophysical data summarized in Table **3**. The emission profiles are broad and featureless with

emission maxima spanning from 544-666 nm. Typically, broad and unstructured emission spectra result from mixed CT states.[5a,6c,17] Complex **1a** emits in the deep red at 666 nm, which is blue shifted by 50 nm from our previous report of 710 nm owing to the use of uncorrected data from a different spectrometer (*vide infra*).[5a] Despite this large hypsochromic shift the remaining compound and optoelectronic characterization is entirely congruent with our previous report and remains one of the reddest-emitting cationic iridium complexes reported to date.[7k,18] The replacement of ppy for dFMeppy results in a blue shift in the emission, with **1b** emitting in the orange at 604 nm. A similar blue shift is observed with replacement of the 2,5-dpp ligand with 2,5-terpy as in **2a**. Combining both the dFMeppy and 2,5-tpy ligands in **2b** results in a green emission of 544 nm.

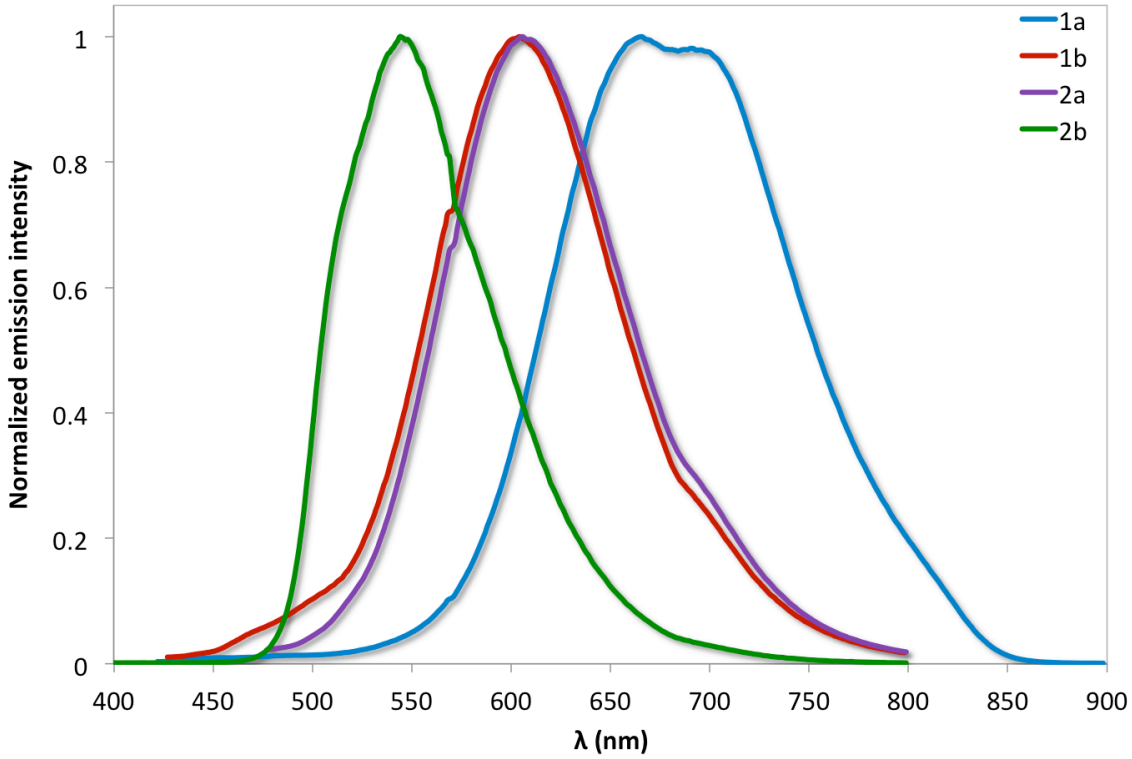

Figure **4**. Steady state uncorrected emission spectra for **1a-2b** in degassed ACN at 298 K.

Table **3**. Relevant photophysical data for complex **1a-2b**

Complex	λ_{em} (nm)[a]	Φ_{PL} (%)[b]	τ_e (μs)[a]	k_r (x10^5 s^{-1})	k_{nr} (x10^5 s^{-1})
1a	666	2.6	0.250 (85.9)[c] and 0.044 (14.0)[c]	1.04[d]	38.9[d]
1b	604	13.1	0.511	2.56	17.0
2a	605	6.3	0.215	2.93	43.5
2b	544	93.0	1.81	5.13	0.386

[a] Measured in deaerated ACN at 298 K. [b] Using $[Ru(bpy)_3](PF_6)_2$ as the standard (Φ_{PL} = 9.5% in deaerated ACN at 298 K)[19]. [c] In parentheses are the relative percentage (%) of each component. [d] k_r and k_{nr} reported only for longer lifetime component of the biexponential decay.

The photoluminescent quantum yield, Φ_{PL}, for **1a** is 2.6%. Though the emission for **1b** and **2a** is essentially isoenergetic, the Φ_{PL} for **1b** of 13.1% is twice that of **2a** (6.3%). These results support the reduced non-radiative vibrations of C-F bonds compared to C-H bonds. Notably, **2b** is extremely brightly, with a Φ_{PL} of 93%, one of the highest photoluminescent quantum yields reported to date! Indeed, there are very few examples of bright green-emitting cationic iridium complexes reported in the literature (cf. Table **4**).

Table **4**. Comparison of the photophysical properties of selected green-emitting cationic iridium complexes.

entry	Complex[a]	$\lambda_{em,\ 298\ K}$ (nm)[b]	Φ_{PL} (%)	Ref
1	$[(dF\text{-}3Meppy)_2Ir(dtBubpy)]^+$	554	62	[6i]
2	$[(dFppy)_2Ir(dtBubpy)]^+$	524	71	[6j]
3	$(3\text{-}CF_3ppy)_2Ir(phen)]^+$	520[c]	65	[6k]

4	$[(4\text{-}MeSO_2ppy)_2Ir(bpy)]^+$	493, 528	64	[6l]
5	$[(dFppy)(ppy)Ir(dtBubpy)]^+$	555	59	[6j]
6	$[Ir(dFppy)_2(SB)]^+$	535	28	[6e]

[a] dF-3MeppyH = 2-(2,4-difluoro-3-methyl)pyridine; dFMeppyH = 2-(2,4-difluorophenyl)-5-methylpyridine; d*t*Bubpy = 4,4'-di-*tert*-butyl-2,2'-bipyridine; 3-CF_3ppy = 2-(3-trifluoromethylphenyl)pyridine; phen = 1,10-phenanthroline; 4-$MeSO_2$ppy = 2-(4-methylsulfonylphenyl)pyridine; bpy = 2,2'-bipyridine; SB = 4,5-diaza-9,9'-spirobifluorene. The counterion for all complexes is PF_6^- [b] recorded in acetonitrile solution; [c] recorded in dichloromethane solution.

The emission lifetime, τ_e, for **1a** was found to be biexponential. However, the long component is similar in magnitude that the monoexponential decays observed for **1b** and **2a**. Interestingly, whereas Bolink[7m] and co-workers reported very short emission lifetimes for $[Ir(ppy)_2(tpy)]PF_6$ of 68 ns and a Φ_{PL} of 1.7% in DCM, the data for **2a** support a much smaller non-radiative rate constant and a photophysically more stable complex. Fluorinated complexes **1b** and **2b** exhibit longer emission lifetimes than their non-fluorinated congeners. Complex **2b** has a τ_e of 1.81 μs, which is nearly ten fold longer than that observed for **2a**. As the emission becomes bluer along the series k_{nr} decreases in concert with the energy gap law while k_r increases.

Theoretical Calculations.

Density functional theory (DFT) and time-dependent DFT (TDDFT) studies were performed to model the geometries and electronic properties of the four complexes in this study.[20] Computations were performed with Gaussian 09[21] using the following DFT protocol at the B3LYP[22] level of theory with the SBKJC-DVZ[23] basis set for iridium, 6-31G* for heavy atoms

directly coordinated to iridium and 3-21G* for all other atoms[23a,24] in the presence of the solvent (ACN).[25]

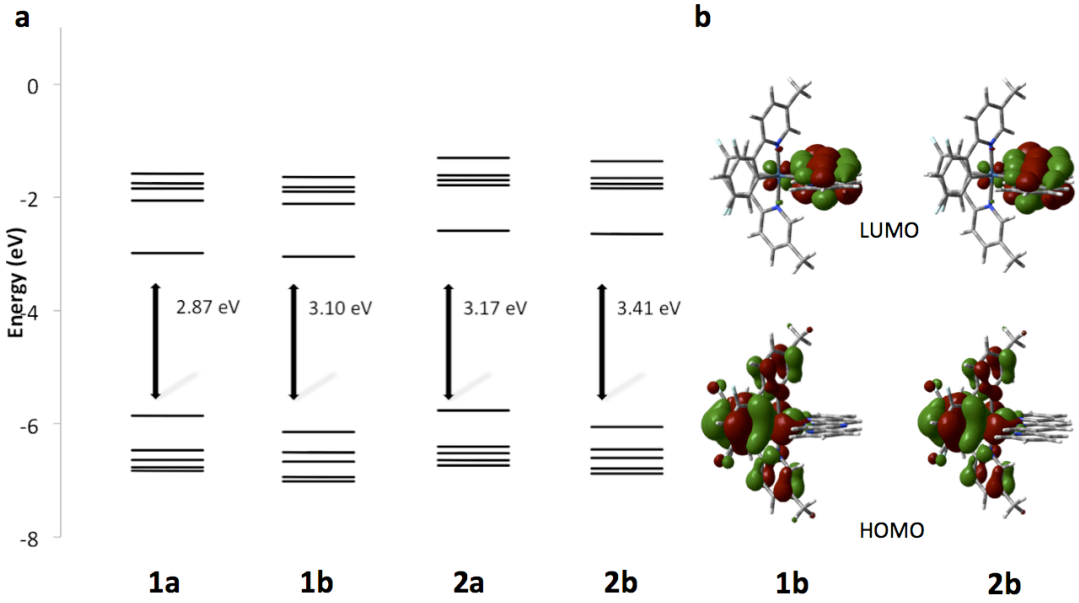

Figure **5**. Calculated energy level scheme for the Kohn-Sham orbitals between HOMO-4 to LUMO+4 of **1a-4b**, and the associated DFT calculated HOMO-LUMO energy gap (in eV) and electron density contour plots for **1a-4a** (0.0004 e bohr^{-3}). The contour plots for **1a** and **2a** mirror those of **1b** and **2b**, respectively.

Figure **5** shows the relative energies of the five highest energy occupied and five lowest energy unoccupied molecular orbitals (MOs) for **1a-2b** along with contour plots of HOMOs and LUMOs for **1b** and **2b** as representative examples. As has been reported for analogous cationic systems,[6c,16d 26] the HOMO is composed of a mixture of π-orbitals located mainly on the aryl ring of the C^N ligands and *d*-orbitals of the iridium atom. The percent contribution from the metal is slightly higher for **1a** and **2a** than it is for **1b** and **2b** (Figure **6**). The LUMO is located almost

exclusively over the entirety of the N^N ligand. Little difference is observed in the relative contributions for these frontier molecule orbitals save for the destabilization of the $\pi^*_{2,5\text{-dpp}}$ LUMO+1 orbital of **1b**, which becomes the LUMO+3 in **2b** (Figure **6**).

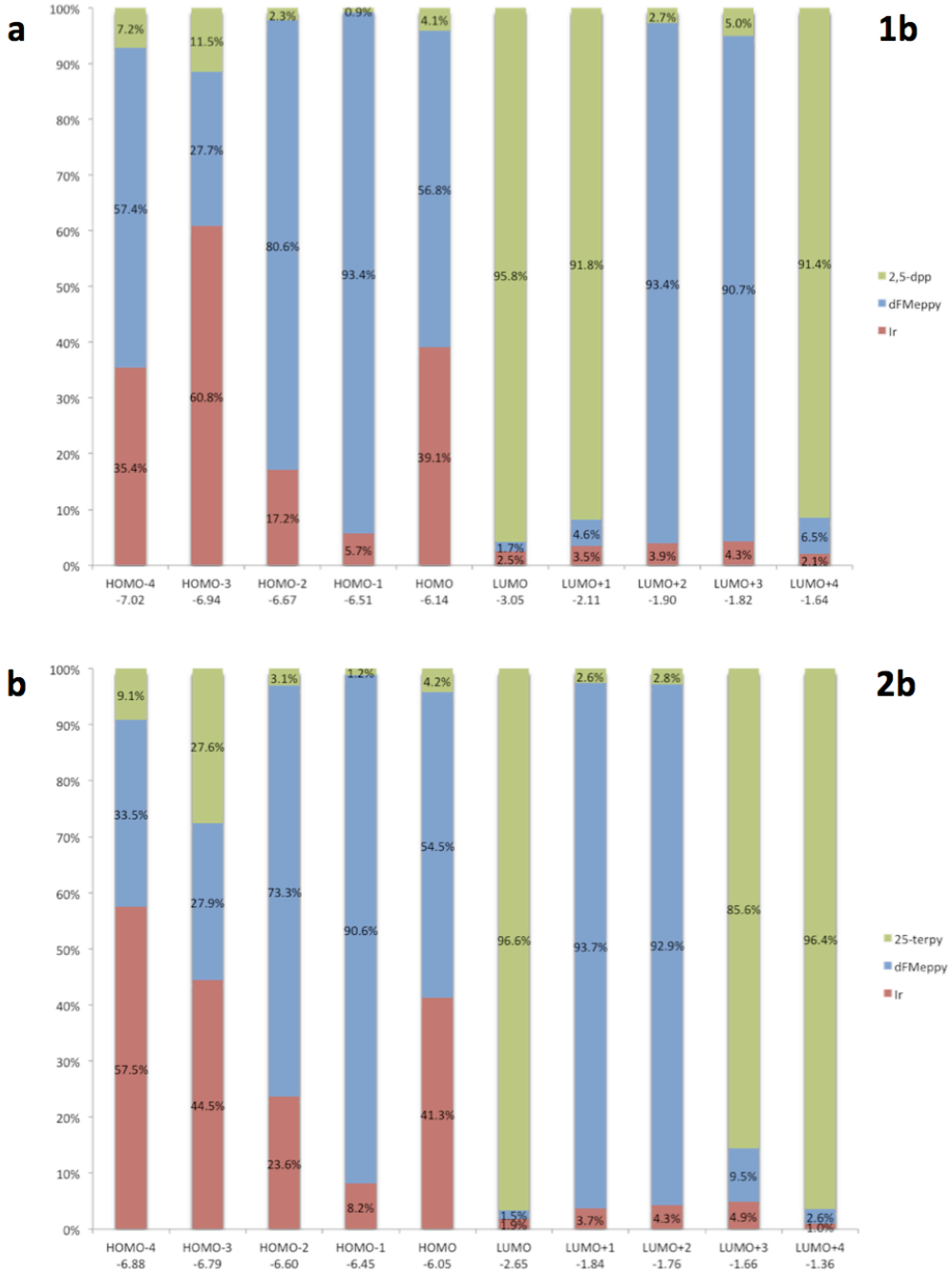

Figure **6**. Orbital energies and percent electron density distribution for HOMO-4 to LUMO+4 for a) **1b** and b) **2b**.

Incorporation of the fluorine atoms onto the C^N ligands stabilizes both the HOMO and the LUMO, with the former to a greater extent. The degree of stabilization is similar for both **1a-b** and **2a-b**. Replacement of the 2,5-dpp ligand in **1a** and **2a** for the 2,5-terpy ligand in **1b** and **2b** results in a significant destabilization of both the HOMO and the LUMO, with the latter to a greater extent. Thus, across the series the HOMO-LUMO gap increases from 2.87 eV to 3.41 eV with **1b** and **2a** possessing coincidentally very similar gaps. These trends mirror those observed for the electrochemical gaps determined by cyclic voltammetry. Further, the UV-visible spectra modeled by TDDFT matches very well those measured in acetonitrile solution as evidenced in Figure **7**. The high intensity feature at around 340 nm was attributed by TDDFT to a mostly ligand-centered (^{1}LC) transition involving the ancillary ligand. The low energy singlet-singlet excitations all exhibit mixed metal-to-ligand (^{1}MLCT) and ligand-to-ligand (^{1}LLCT) charge transfer character.

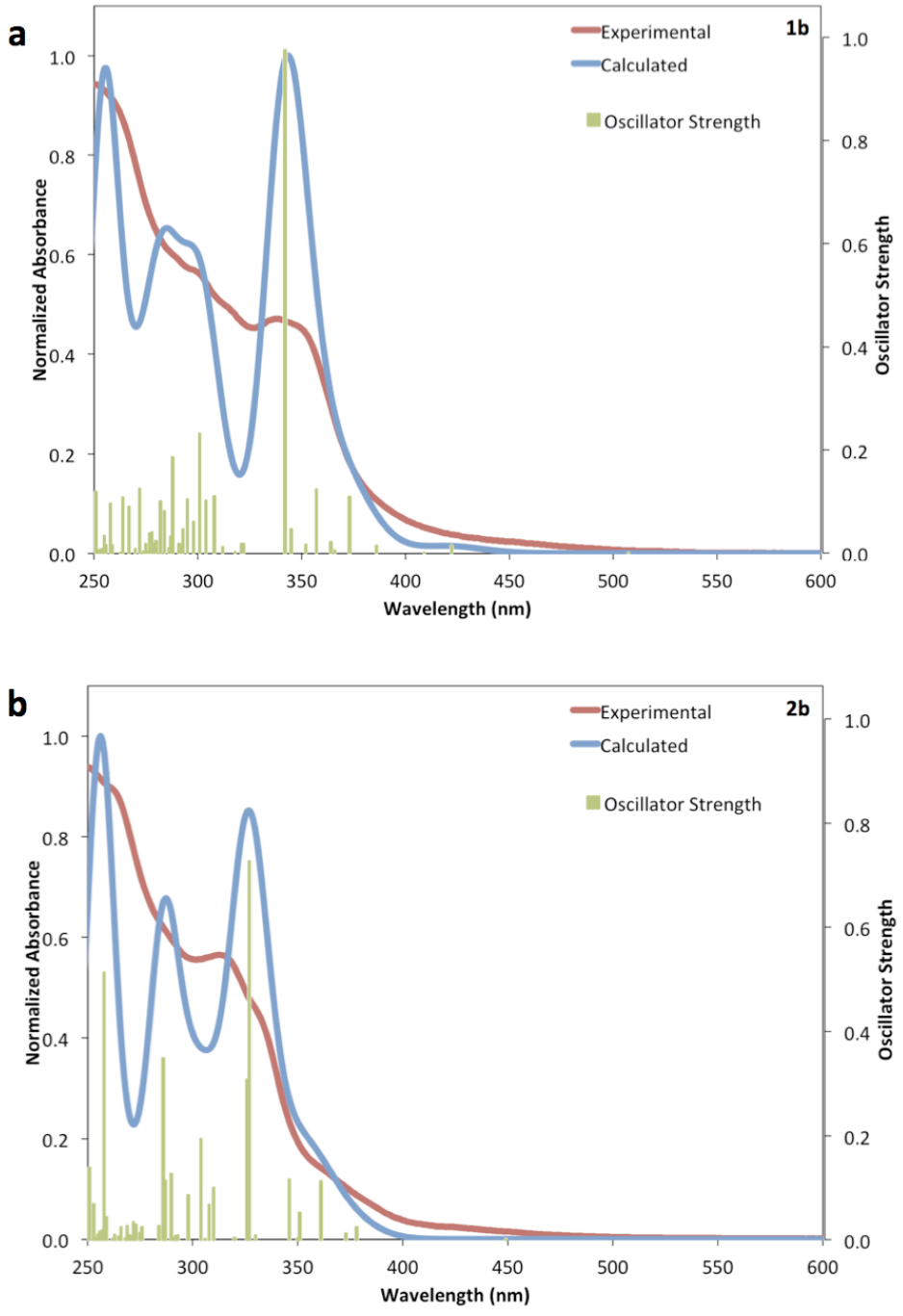

Figure **7**. Experimental (red) and calculated UV-Vis spectrum (blue – fwhm = 1000 cm^{-1}) obtained from TDDFT calculations with the corresponding vertical excitations (green).

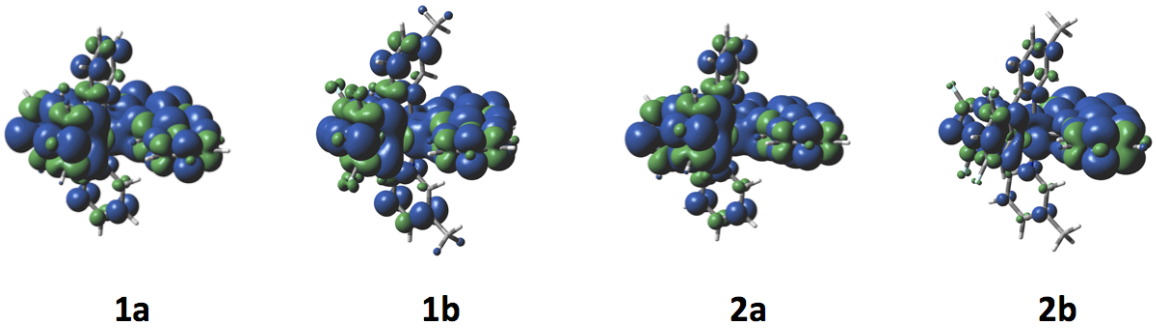

Figure **8**. Calculated spin density contours of the T_1 state for **1a**, **2a**, **3a** and **4a** (isocontour value of 0.0004 au).

The nature of lowest energy triplet state (T_1) for **1a-2b** was calculated using spin-unrestricted UB3LYP after optimization of the geometry. The spin densities for the T_1 state for **1a-2b** are shown in Figure **8**. The topologies of the spin densities for **1a**, **1b** and **2a** perfectly match the superposition of the topologies of the electron densities of their respective HOMO and LUMO, strongly suggesting that the emissive state is mixed ^{3}CT in nature. TDDFT calculations support this assignment and attribute the T_1 state for these three complexes to a LUMO→HOMO transition. Indeed, the observed broad and unstructured emission at 298 K in ACN corroborates the computational picture. The spin density for **2b** is relatively more localized on the 2,5-terpy ligand, suggesting an increased ^{3}LC contribution to the ^{3}CT T_1 state. TDDFT calculations described a T_1 state consisting of three transitions: LUMO→HOMO-5 (12%), LUMO→HOMO-3 (21%) and LUMO→ HOMO (59%), supporting this complex assignment. The emission spectra obtained at 298 K however remained unstructured and thus the ^{3}LC contribution must be minor.

The emission energy was ascertained using three different methodologies and these results are summarized in Table **5**. The calculated adiabatic energy was determined as the difference

between the T_1 and S_0 states in their respective optimized geometries (E_{AE}). The emission energies predicted by TDDFT (E_{TDDFT}) for the $S_0 \rightarrow T_1$ monoexcitation are based on the optimized S_0 geometry and result from a spin-restricted calculation. The emission at 298 K was computed (E_{em}) from the vertical energy difference between the T_1 and S_0 states at the optimized geometry of the T_1 state.[6i] The calculations match to within 3.4% relative error the experimental emission measured at 298 K.

Table **5**. Predicted Emission Energies

	Theoretical[a]				
	E_{TDDFT} /nm	E_{AE} /nm	E_{em} /nm	λ_{em} (298 K) /nm	Error[b] /%
1a	568	602	682	666	2.2
1b	514	537	595	604	1.5
2a	496	523	585	605	3.4
2b	459	477	548	544	0.8

[a] E_{TDDFT} = energy of $S_0 \rightarrow T_1$ transition obtained by TDDFT at the S_0 optimized geometry; $E_{0,0} = E(T_1)-E(S_0)$ at their respective optimized geometries obtained by DFT; $E_{AE} = E(T_1)-E(S_0)$ at the T_1 optimized geometries (adiabatic electronic emission) obtained by DFT. All values obtained are in the presence of ACN solvent; [b] Error = $|\lambda_{em}(298K)-E_{em}/\lambda_{em}(298K)|$ in eV.

Device Characterization

Electroluminescent devices of layering Al/LiF/iTMC/PEDOT:PSS/ITO were tested at constant current under nitrogen atmosphere in a glovebox. Complexes **1a** and **2a** yielded electroluminescent devices of appreciable brightness and stability. However, the devices from

the fluorinated complexes **1b** and **2b** were highly unstable and short-lived and so their electroluminescence properties beyond their EL spectra are not presented.

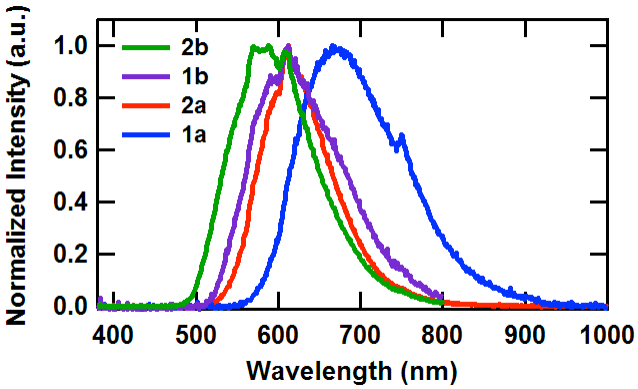

Figure **9**. Electroluminescence from Al/LiF/iTMC/PEDOT:PSS/ITO devices for iTMCs based on **1a**, **1b**, **2a** and **2b**. Devices were driven at a constant current of 1.5 mA.

In Figure **9** we show the electroluminescence (EL) spectra of the **1a**, **1b**, **2a**, and **2b** LEEC devices. The EL emission maximum of **1a** is 666 nm and **1b** is 612 nm, while the EL spectrum of **2a** peaks at 611 nm and **2b** at 588 nm. Thus, for each complex the EL spectrum closely matches the PL spectrum. Commission Internationale de l'Éclairage (CIE) coordinates of **2a** are (0.595, 0.404), that is, along the spectral locus between the green and red primaries. The device of complex **1a** exhibits CIE coordinates of (0.681, 0.328), very close to the saturated red primary and among the reddest iridium iTMC devices to date. This deep red emission compared to standard Ir complexes such as $[(ppy)_2Ir(bpy)]^+$ is attributed to the increased conjugation and electron withdrawing character of the substituents on the N^N ligand.

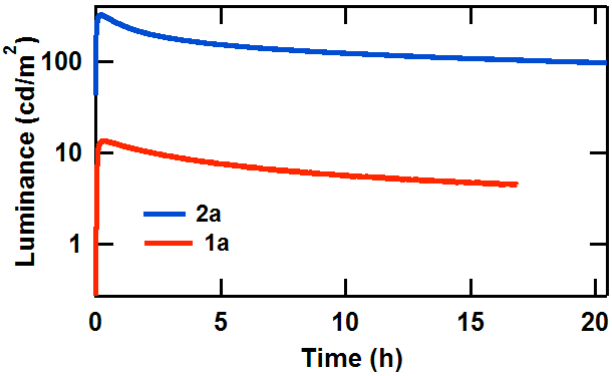

Figure **10**. The luminance versus time for Al/LiF/iTMC/PEDOT:PSS/ITO devices for iTMCs **1a** and **2a**.

The luminance versus time characteristics of the electroluminescent devices employing **1a** and **2a** as emitters under constant current driving (current density 0.5 mA/mm^2) are given in Figure **10**. These devices show intrinsically fast turn-on times, that is, the time to maximum luminance, L_{max}. Device **2a** reaches a maximum luminance of 324 cd/m^2 in 11 min, while **1a** achieves 14 cd/m^2 in 19 min. These are relatively fast responses among intrinsic iridium complexes, which can require hours to days to reach L_{max} under constant current or constant voltage driving.[3c] The luminescent half-lives of these devices, the time to decay from L_{max} to $\frac{1}{2}L_{max}$, are 380 min and 250 min for **1a** and **2a**, respectively. The external quantum efficiency (EQE) data of **1a** and **2a** electroluminescent devices is presented in Figure **11**. Complex **2a** complex gives a peak photons/electron ratio of 0.37%, while **1a** achieves a maximum of 0.08%. The higher performance of the **2a** device compared to the **1a** device and the better device performance of the **a** complexes over the **b** complexes (data not shown) correlates with the trend of the HOMO levels: **2a** (-5.76 eV) < **1a** (-5.86 eV) < **1b** (-6.05 eV) < **2b** (-6.14 eV). That is, **2a** has the lowest oxidation potential and facilitates more efficient hole injection. This would

suggest that hole injection is the limiting factor in these devices, plausible considering the offset between the HOMO of each complex and the work function of PEDOT films (4.7-5.4 eV).[27] Overall, the strategy of extending conjugation of the N^N ligand of iridium iTMCs produces devices with appreciable luminance and lifetime and red-shifted electroluminescence.

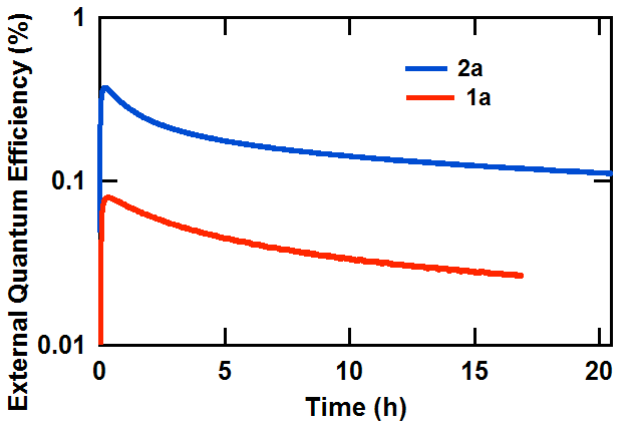

Figure **11**. The external quantum efficiency versus time for Al/LiF/iTMC/PEDOT:PSS/ITO devices for iTMCs **1a** and **2a**.

Conclusions.

In this study, we reported the synthesis of four cationic iridium complexes and we investigated their optoelectronic properties. Complex **1a** was found to be a deep red emitter in acetonitrile solution while complex **2b** was a very bright green emitter (Φ_{PL} = 93%); complexes **1b** and **2a** were orange emitters. These complexes were integrated into LEEC devices. While the devices incorporating the fluorinated complexes **1b** and **2b** proved to highly unstable, devices based on **1a** and **1b** resulted in deep red and orange-red emission with stabilities of 380 and 250 minutes, respectively. Notably, the LEEC with **1a**, possessing CIE coordinates of (0.681, 0.328), is very close to the saturated red primary and among the reddest iridium iTMC devices to date.

Acknowledgements. EZ-C acknowledges CFI (Canadian Foundation for Innovation), NSERC (the Natural Sciences and Engineering Research Council of Canada), FQRNT (Le Fonds québécois de la recherche sur la nature et les technologies) and the University of St Andrews for financial support. We acknowledge Prof. Garry Hanan for providing access to facilities at the Université de Montréal.

Experimental Section

General Synthetic Procedures. Commercial chemicals were used as supplied. All reactions were performed using standard Schlenk techniques under inert (N_2) atmosphere with freshly distilled anhydrous solvents obtained from a Pure MBRAUN (MB-SPS) purification system except where specifically mentioned. Flash column chromatography was performed using silica gel (Silia-P from Silicycle, 60 Å, 40-63 μm). Analytical thin layer chromatography (TLC) was performed with silica plates with aluminum backings (250 μm with indicator F-254). Compounds were visualized under UV light. ^{1}H. ^{19}F and ^{13}C NMR spectra were recorded on a Brucker Avance 400 spectrometer at 400 MHz, 376 MHz and 100 MHz, respectively. The following abbreviations have been used for multiplicity assignments: “s” for singlet, “d” for doublet, “t” for triplet, “m” for multiplet and “br” for broad. Deuterated dimethylsulfoxide (DMSO-d_6), deuterated chloroform ($CDCl_3$) and deuterated actonitrile (CD_3CN) were used as the solvent of record. Melting points (Mp’s) were recorded using open-ended capillaries on a Meltemp melting point apparatus and are uncorrected. High resolution mass spectra were recorded on a quadrupole time-of-flight (ESI-Q-TOF), model MICROTOF II from Bruker in positive electrospray ionization mode at the Université de Montreal. The corresponding

iridium(III) dimers, $[(C^N)_2Ir(Cl)]_2$ were prepared according to the literature, where C^N is 2-phenylpyridinato or 2-(2,4-difluorophenyl)pyridinato.[28]

General Procedure for the Synthesis of ancillary (N^N) ligands.

2,5-Di(pyridin-2-yl)pyrazine (2,5-dpp). The synthesis was run analogous to our previsouly reported protocol but using 4.35 mmol of 2-bromopyridine.[8]

Beige solid. **Yield:** 54%. **R_f:** 0.25 (DCM/Acetone 90/10; Silica). **Mp:** 190-193 °C (Lit. Mp.[8]: 186-190 °C). **^{1}H NMR (400 MHz, DMSO-d_6) δ (ppm):** 9.63 (s, 2H), 8.79 (d, J = 4.7 Hz, 2H), 8.43 (d, J = 7.9 Hz, 2H), 8.04 (td, J = 7.6, 1.6 Hz, 2H), 7.57 (dd, J = 7.5, 5.0 Hz, 2H). **^{13}C NMR (100 MHz, DMSO-d_6) δ (ppm):** 161.09, 148.56, 147.01, 140.24, 136.60, 123.91, 119.95. HR-MS (ES-Q-TOF) ($C_{14}H_{11}N_4Na^+$) Calculated: 257.0798; Experimental: 257.0797. The ^{1}H NMR is in agreement with that previously reported with slight differences in chemical shifts due to the change in NMR solvent from ACN-d_3 to DMSO-d_6.[8]

2,2':5',2"-terpyridine (2,5-tpy). 1.6 M *n*-BuLi (0.58 mL, 0.93 mmol, 2.2 equiv.) was added drop wise over 10 min to a suspension of 2-bromopyridine (0.147 g, 0.93 mmol, 2.2 equiv.) in 10 mL of dry THF under nitrogen atmosphere at -78°C. The reaction was stirred 30 minutes and a mixture of $ZnCl_2$ (1.26 g, 9.28 mmol, 2.2 equiv.) in 10 mL of dry THF was added via cannula. The mixture was then stirred 2 hours at room temperature and added via cannula to a mixture of 2,5-dibromopyridine (0.100 g, 0.42 mmol, 1.0 equiv.) and $Pd(PPh_3)_4$ (0.048 g, 10 mol%) in 10 mL of dry THF at room temperature. The mixture was stirred under nitrogen overnight at 65 °C. The solid was filtered, washed several times with Et_2O and dissolved in 30 mL of saturated EDTA and 15 mL of saturated Na_2CO_3 in water. The mixture was stirred for 1 h and the solid

was filtered, washed several times with water and dried over reduced pressure to obtain a a brownish solid. The crude product was purified by alumina column using hexane/ethylacetate (7:3) and isolated 71 mg of beige solid that was found to be analytically pure.

Beige solid. **Yield:** 72%. **R_f:** 0.35 (DCM/Acetone 90/10; Silica). **Mp:** 139-141°C (Lit. Mp[29]: 182-184 °C). **^{1}H NMR (400 MHz, $CDCl_3$) δ:** 9.30 (dd, *J* = 2.3, 0.9 Hz, 1H), 8.77 (dt, *J* = 4.8, 1.5 Hz, 1H), 8.73 (ddd, *J* = 4.8, 1.8, 0.9 Hz, 1H), 8.54 (dd, *J* = 8.3, 0.9 Hz, 1H), 8.51 – 8.47 (m, 2H), 7.89 – 7.86 (m, 1H), 7.85 – 7.82 (m, 2H), 7.37 – 7.30 (m, 2H). **^{13}C NMR (101 MHz, $CDCl_3$) δ**: 156.65, 156.20, 155.09, 150.52, 149.67, 148.09, 137.35, 135.62, 135.06, 124.25, 123.25, 121.73, 121.35, 121.02.**HR-MS (ES-Q-TOF) ($C_{15}H_{11}N_3Na^+$) Calculated:** 256.0851; **Experimental:** 256.0854. The ^{1}H NMR is in agreement with that previously reported with slight differences in chemical shifts due to the change in NMR solvent from $CDCl_3$ to DMSO-d_6.[9,29]

General procedure for the synthesis of $[(C^N)_2Ir(N^N)]PF_6$ complexes. Iridium dimer (0.07 mmol, 1.0 equiv.) and N^N ligand (2,5-dpp or 2,5-tpy) (0.16 mmol, 2.21 equiv.) were solubilized with 12 mL of 2-ethoxyethanol to reach a concentration in iridium of 0.04 M. The mixture was degassed by multiple vacuum and N_2 purging cycles. The suspension was heated at 130 °C for 24 h. The reaction mixture was cooled to room temperature and diluted with water. The aqueous suspension was washed several times with Et_2O. The aqueous layer was heated at 70 °C for 15 min and cooled back down to room temperature. A solution of NH_4PF_6 (10 equiv., 1.0 g / 10 mL) was added drop by drop to the aqueous phase to cause the precipitation of a solid. The suspension was cooled to 0 °C for 1 h, filtered and the resulting solid was washed with cold water. The crude solid was purified by flash chromatography on silica gel using DCM to DCM/Acetone (9/1) or DCM + 5% NEt_3 to DCM/Acetone (9/1) + 5% NEt_3.

[(ppy)$_2$Ir(2,5-dpp)](PF$_6$), 1a. Red solid. **Yield:** 48 %. **Mp:** 243−247 °C. **R$_f$:** 0.20 (DCM/Acetone 90/10; Silica). **^{1}H NMR (400 MHz, Acetonitrile-d_3) δ (pmm):** 9.77 (s, 1H), 8.99 (s, 1H), 8.72 (d, *J* = 8.2 Hz, 1H), 8.52 (d, *J* = 4.9 Hz, 1H), 8.44 (d, *J* = 8.0 Hz, 1H), 8.21 (t, *J* = 7.9 Hz, 1H), 8.10 (dd, *J* = 8.2, 3.8 Hz, 2H), 8.05 (d, *J* = 5.5 Hz, 1H), 7.98 (td, *J* = 7.7, 1.7 Hz, 1H), 7.87 (ddd, *J* = 12.1, 7.2, 4.2 Hz, 4H), 7.79 (d, *J* = 5.8 Hz, 1H), 7.65 – 7.60 (m, 2H), 7.47 (dd, *J* = 7.6, 4.8 Hz, 1H), 7.16 – 7.11 (m, 1H), 7.10 – 7.01 (m, 4H), 7.00 – 6.94 (m, 1H), 6.36 (d, *J* = 7.6 Hz, 1H), 6.27 (d, *J* = 7.6 Hz, 1H). **^{13}C NMR (101 MHz, CD$_3$CN) δ (ppm):** 166.91, 154.76, 151.52, 150.77, 149.77, 149.44, 149.38, 149.22, 148.55, 144.73, 143.87, 143.53, 141.70, 139.18, 138.49, 138.43, 137.44, 131.26, 130.95, 130.17, 128.66, 125.73, 124.66, 124.60, 124.55, 123.36, 123.26, 122.63, 122.55, 121.77, 119.68, HR-MS (ES-Q-TOF): **[M-PF$_6$]$^+$** ($C_{36}H_{26}N_6Ir$+) Calculated: 735.1848; Experimental: 735.1882. The compound characterization is in agreement with that previously reported with slight differences in chemical shifts due to the change in NMR solvent from acetone-d_6 to acetonitrile-d_3.[8]

[(dFMeppy)$_2$Ir(2,5-dpp)](PF$_6$), **1b**. Dark brown solid. **Yield:** 35%. **Mp:** 234−236 °C. **R$_f$:** 0.15 (DCM/Acetone 80/20; Silica). **^{1}H NMR (400 MHz, Acetonitrile-d_3) δ (ppm):** 9.79 (s, 1H), 8.95 (s, 1H), 8.73 (d, *J* = 8.2 Hz, 1H), 8.60 (d, *J* = 4.8 Hz, 1H), 8.46 (d, *J* = 7.8 Hz, 1H), 8.24 (t, *J* = 7.9 Hz, 4H), 8.06 (d, *J* = 5.5 Hz, 1H), 7.99 (t, *J* = 8.0 Hz, 1H), 7.77 (t, *J* = 7.7 Hz, 2H), 7.61 (d, *J* = 7.3 Hz, 2H), 7.50 (dd, *J* = 7.5, 4.8 Hz, 1H), 7.41 (s, 1H), 6.82 – 6.70 (m, 2H), 5.84 (dd, *J* = 8.4, 2.5 Hz, 1H), 5.73 (dd, *J* = 8.9, 2.4 Hz, 1H), 2.16 (s, 3H), 2.15 (s, 3H). **^{19}F NMR (376 MHz, Acetone-d$_6$) δ (ppm):** -73.03 (d, *J* = 707.4 Hz), -108.48 – -109.04 (m), -110.90 – -111.55 (m). **^{13}C NMR (100 MHz, Acetone-d$_6$) δ (ppm):** 164.34, 164.23, 161.84, 161.74, 159.04, 158.91,

156.53, 156.40, 153.32, 147.15, 147.09, 141.84, 135.63, 135.34, 129.91, 129.89, 129.68, 128.76, 128.69, 124.00, 122.53, 122.47, 120.79, 120.69, 116.22, 116.03, 98.65, 9.38, 98.14, 56.28, 55.91. **HR-MS (**ES-Q-TOF**): [M-PF_6]$^+$ Calculated:** ($C_{38}H_{26}IrN_6F_4^+$) 835.1784; **Found:** 835.1824.

[$(ppy)_2$Ir(2,5-tpy)](PF_6), 2a. Orange red solid. **Yield:** 80%. **Mp:** 225-227 °C. **R_f:** 0.20 (DCM/Acetone 90/10; Silica). **^{1}H NMR (400 MHz, Acetonitrile-d_3) δ (ppm)**: 8.74 – 8.67 (m, 2H), 8.65 – 8.56 (m, 3H), 8.17 (td, *J* = 7.9, 1.6 Hz, 1H), 8.09 (tt, *J* = 6.6, 1.1 Hz, 2H), 8.04 (ddd, *J* = 5.5, 1.6, 0.8 Hz, 1H), 7.90 – 7.82 (m, 5H), 7.75 (ddd, *J* = 5.9, 1.5, 0.8 Hz, 1H), 7.69 – 7.62 (m, 2H), 7.54 (ddd, *J* = 7.7, 5.4, 1.2 Hz, 1H), 7.39 (ddd, *J* = 7.7, 4.8, 1.1 Hz, 1H), 7.13 – 7.02 (m, 4H), 6.97 (dtd, *J* = 10.3, 7.4, 1.4 Hz, 2H), 6.38 – 6.31 (m, 2H). **^{13}C NMR (100 MHz, Acetonitrile-d_3) δ (ppm):** 167.13, 155.20, 151.30, 150.38, 149.94, 149.17, 149.01, 148.68, 143.82, 143.76, 139.08, 138.40, 138.22,137.31, 136.24, 131.27, 131.21, 128.11, 124.56, 124.23, 124.05, 123.21, 123.18, 122.37, 122.25, 120.76, 119.60, 119.53, 116.99. **HR-MS (**ES-Q-TOF**): [M-PF_6]$^+$ Calculated:** ($C_{37}H_{27}IrN_5$) 734.1892; **Found:** 734.1849.

[$(dFMeppy)_2$Ir(2,5-tpy)](PF_6), **2b.** Light greenish solid. **Yield:** 85%. **Mp**: 208-210 °C. **R_f:** 0.25 (DCM/Acetone 90/10; Silica). **^{1}H NMR (400 MHz, Acetonitrile-d_3)** δ **(ppm):** 8.77 (dd, *J* = 8.6, 2.1 Hz, 1H), 8.68 – 8.67 (m, 1H), 8.67 – 8.59 (m, 3H), 8.26 – 8.19 (m, 3H), 8.04 (ddd, *J* = 5.6, 1.6, 0.8 Hz, 1H), 7.89 (td, *J* = 7.8, 1.8 Hz, 1H), 7.75 (dddd, *J* = 7.9, 5.6, 3.7, 1.5 Hz, 3H), 7.59 – 7.56 (m, 1H), 7.55 (dq, *J* = 2.0, 1.2 Hz, 1H), 7.45 (d, *J* = 1.9 Hz, 1H), 7.41 (ddd, *J* = 7.6, 4.8, 1.1 Hz, 1H), 6.73 (dddd, *J* = 12.8, 11.7, 9.4, 2.4 Hz, 2H), 5.84 (dd, *J* = 8.7, 2.4 Hz, 1H), 5.77 (dd, *J* = 8.7, 2.4 Hz, 1H), 2.14 (s, 3H), 2.13 (s, 3H). **^{19}F NMR (376 MHz, Acetonitrile-d_3) δ (ppm):** -74.13 (d, *J* = 706.3 Hz), -110.20 (dq, *J* = 98.5, 9.6 Hz), -112.16 (t, *J* = 11.5 Hz). **^{13}C NMR (100**

MHz, Acetonitrile-d_3) δ (ppm): 160.65, 155.08, 153.53, 153.22, 150.62, 149.91, 149.06, 148.89, 148.70, 139.90, 139.40, 138.48, 137.30, 136.55, 134.34, 128.27, 127.82, 124.94, 124.63, 124.14, 122.88, 122.78, 120.93, 117.02, 113.73, 113.53, 113.37, 98.60, 98.33, 98.06, 16.82. **HR-MS (**ES-Q-TOF**): $[M\text{-}PF_6]^+$ Calculated:** ($C_{39}H_{27}IrF_4N_5$) 834.1828; **Found:** 834.1838.

Photophysical measurements. All samples were prepared in HPLC grade acetonitrile (ACN) with varying concentrations on the order of μM. Absorption spectra were recorded at RT using a Cary 500i double beam spectrophotometer. Molar absorptivity determination was verified by linear least-squares fit of values obtained from at least three independent solutions at varying concentrations with absorbance ranging from 6.88×10^{-1} to 3.19×10^{2} μM.

The sample solutions for the emission spectra were prepared in Ar-degassed dry ACN. Emission spectra were recorded at room temperature using a Cary Eclipse 300 fluorimeter. The samples were excited at the absorption maxima of the dominant low-energy ^{1}MLLCT band as indicated in Table **2**. Excited state lifetimes were measured with an Edinburgh Instruments Mini Tau lifetime fluorimeter with an EPL 405 laser (exciting at 405 nm). Melting points were measured with a BI Barnsted Electrothermal 9100 apparatus and were quoted referencing the decomposition temperature. Emission quantum yields were determined using the optically dilute method.[30] A stock solution with absorbance of ca. 0.5 was prepared and then four dilutions were prepared with dilution factors of 40, 20, 13.3 and 10 to obtain solutions with absorbances of ca. 0.013 0.025, 0.038 and 0.05, respectively. The Beer-Lambert law was found to be linear at the concentrations of the solutions. The emission spectra were then measured after the solutions were rigorously degassed with solvent-saturated argon gas (Ar) for 20 minutes prior to spectrum

acquisition using septa-sealed quartz cells from Starna. For each sample, linearity between absorption and emission intensity was verified through linear regression analysis and additional measurements were acquired until the Pearson regression factor (R^2) for the linear fit of the data set surpassed 0.9. Individual relative quantum yield values were calculated for each solution and the values reported represent the slope value. The equation $\Phi_s = \Phi_r(A_r/A_s)(I_s/I_r)(n_s/n_r)^2$ was used to calculate the relative quantum yield of each of the sample, where Φ_r is the absolute quantum yield of the reference, *n* is the refractive index of the solvent, *A* is the absorbance at the excitation wavelength, and *I* is the integrated area under the corrected emission curve. The subscripts s and r refer to the sample and reference, respectively. A solution of $[Ru(bpy)_3](PF_6)_2$ in ACN ($\Phi r = 0.095$) was used as the external reference.[19]

Electrochemistry measurements. Cyclic voltammetry (CV) measurements were performed in argon-purged purified acetonitrile at room temperature with a BAS CV50W multipurpose equipment interfaced to a PC. Solutions for cyclic voltammetry were prepared in ACN and degassed with ACN-saturated argon bubbling for about 20 min prior to scanning. Tetra(*n*-butyl)ammoniumhexafluorophosphate ($TBAPF_6$; ca. 0.1 M in ACN) was used as the supporting electrolyte. A non-aqueous Ag/Ag^+ electrode (silver wire in a solution of 0.1 M $AgNO_3$ in ACN) was used as the pseudoreference electrode; a glassy-carbon electrode was used for the working electrode and a Pt electrode was used as the counter electrode. The reference was set using an internal 1 mM ferrocene/ferrocinium sample at 380 mV vs SCE in acetonitrile. The redox potentials are reported relative to a standard calomel electrode (SCE) with a ferrocenium/ferrocene (Fc^+/Fc) redox couple as an internal reference (0.38 V vs SCE).[11]

Device Fabrication. Indium Tin Oxide (ITO) substrates (Thin Film Devices) were first cleaned by hand scrubbing with non-ionic soap and water and then further cleaned in an ultrasonic water bath. Subsequently, the substrates were subjected to UV ozone cleaning for 10 minutes. PEDOT:PSS (Clevios AI 4083) solutions were filtered through a 0.45 μm filter and then spin coated onto ITO substrates to reach a target thickness of 90 to 100 nm. The PEDOT:PSS films were baked at 100 ºC for 10 minutes to remove water. Samples were then transferred into a nitrogen glove box with oxygen and water levels lower than 1 ppm for the remaining steps. All iTMCs were dissolved in acetonitrile at a concentration of 24 mg/mL and heated at 80 ºC for 10 minutes. These solutions were passed through a 0.1 μm filter and spin coated onto the PEDOT:PSS covered ITO substrates, yielding active layer thicknesses of around 100 nm. Following this, the samples were baked at 120 ºC for 60 min to remove solvent. Samples were transferred into a thermal evaporator to deposit 1 nm of LiF and 80 nm of Al through a shadow mask to define twelve devices each with a 3 mm^2 area. A 760D electrochemical analyzer from CH Instruments (Austin, TX) was used for electrical testing. Radiant flux measurements were obtained with a calibrated Labsphere integrating sphere and photodiode, with photocurrents measured with a Keithley 6485 Picoammeter. An Ocean Optics Jazz spectrometer was used to measure the electroluminescence.

References

(1) (a) Slinker, J. D.; Rivnay, J.; Moskowitz, J. S.; Parker, J. B.; Bernhard, S.; Abruña, H. D.; Malliaras, G. G. *J. Mater. Chem.* **2007**, *17*, 2976; (b) Costa, R. D.; Ortí, E.; Bolink, H. J.; Monti, F.; Accorsi, G.; Armaroli, N. *Angew. Chem. Int. Ed.* **2012**, *51*, 8178.
(2) (a) Pei, Q.; Yu, G.; Zhang, C.; Yang, Y.; Heeger, A. J. *Science* **1995**, *269*, 1086; (b) Pei, Q.; Yang; Yu, G.; Zhang, C.; Heeger, A. J. *J. Am. Chem. Soc.* **1996**, *118*, 3922.
(3) (a) Maness, K. M.; Masui, H.; Wightman, R. M.; Murray, R. W. *J. Am. Chem. Soc.* **1997**, *119*, 3987; (b) Lowry, M. S.; Bernhard, S. *Chem. Eur. J.* **2006**, *12*, 7970; (c) Hu, T.; He, L.; Duan, L.; Qiu, Y. *J. Mater. Chem.* **2012**, *22*, 4206.

(4) (a) Shen, Y.; Kuddes, D. D.; Naquin, C. A.; Hesterberg, T. W.; Kusmierz, C.; Holliday, B. J.; Slinker, J. D. *Appl. Phys. Lett.* **2013**, *102*, 203305; (b) deMello, J. C. *Physical Review B* **2002**, *66*, 235210; (c) Slinker, J. D.; DeFranco, J. A.; Jaquith, M. J.; Silveira, W. R.; Zhong, Y.-W.; Moran-Mirabal, J. M.; Craighead, H. C.; Abruña, H. D.; Marohn, J. A.; Malliaras, G. G. *Nat. Mater.* **2007**, *6*, 894; (d) Pingree, L. S. C.; Rodovsky, D. B.; Coffey, D. C.; Bartholomew, G. P.; Ginger, D. S. *J. Am. Chem. Soc.* **2007**, *129*, 15903; (e) Rodovsky, D. B.; Reid, O. G.; Pingree, L. S. C.; Ginger, D. S. *ACS Nano* **2010**, *4*, 2673; (f) van Reenen, S.; Matyba, P.; Dzwilewski, A.; Janssen, R. A. J.; Edman, L.; Kemerink, M. *J. Am. Chem. Soc.* **2010**, *132*, 13776.
(5) (a) Lowry, M. S.; Hudson, W. R.; Pascal Jr., R. A.; Bernhard, S. *J. Am. Chem. Soc.* **2004**, *126*, 14129; (b) Chi, Y.; Chou, P.-T. *Chem. Soc. Rev.* **2010**, *39*, 638; (c) Ladouceur, S.; Zysman-Colman, E. *Eur. J. Inorg. Chem.* **2013**, *2013*, 2985.
(6) (a) Lowry, M. S.; Goldsmith, J. I.; Slinker, J. D.; Rohl, R.; Pascal, R. A.; Malliaras, G. G.; Bernhard, S. *Chem. Mater.* **2005**, *17*, 5712; (b) Lafolet, F.; Welter, S.; Popovic, Z.; De Cola, L. *J. Mater. Chem.* **2005**, *15*, 2820; (c) Tamayo, A. B.; Garon, S.; Sajoto, T.; Djurovich, P. I.; Tsyba, I. M.; Bau, R.; Thompson, M. E. *Inorg. Chem.* **2005**, *44*, 8723; (d) Bolink, H. J.; Cappelli, L.; Coronado, E.; Parham, A.; Stossel, P. *Chem. Mater.* **2006**, *18*, 2778; (e) Su, H.-C.; Fang, F.-C.; Hwu, T.-Y.; Hsieh, H.-H.; Chen, H.-F.; Lee, G.-H.; Peng, S.-M.; Wong, K.-T.; Wu, C.-C. *Adv. Funct. Mater.* **2007**, *17*, 1019; (f) Lo, K. K.-W.; Lee, P.-K.; Lau, J. S.-Y. *Organometallics* **2008**, *27*, 2998; (g) He, L.; Qiao, J.; Duan, L.; Dong, G.; Zhang, D.; Wang, L.; Qiu, Y. *Adv. Funct. Mater.* **2009**, *19*, 2950; (h) Shan, G.-G.; Li, H.-B.; Cao, H.-T.; Zhu, D.-X.; Su, Z.-M.; Liao, Y. *J. Organomet. Chem.* **2012**, *713*, 20; (i) Tordera, D.; Serrano-Pérez, J. J.; Pertegás, A.; Ortí, E.; Bolink, H. J.; Baranoff, E.; Nazeeruddin, M. K.; Frey, J. *Chem. Mater.* **2013**, *25*, 3391; (j) Tordera, D.; Delgado, M.; Ortí, E.; Bolink, H. J.; Frey, J.; Nazeeruddin, M. K.; Baranoff, E. *Chem. Mater.* **2012**, *24*, 1896; (k) Shavaleev, N. M.; Scopelliti, R.; Grätzel, M.; Nazeeruddin, M. K.; Pertegás, A.; Roldán-Carmona, C.; Tordera, D.; Bolink, H. J. *J. Mater. Chem. C* **2013**, *1*, 2241; (l) Constable, E. C.; Ertl, C. D.; Housecroft, C. E.; Zampese, J. A. *Dalton Trans.* **2014**, DOI: 10.1039/c3dt53626b.
(7) (a) Neve, F.; Crispini, A.; Campagna, S.; Serroni, S. *Inorg. Chem.* **1999**, *38*, 2250; (b) Cunningham, G. B.; Li, Y.; Liu, S.; Schanze, K. S. *J. Phys. Chem. B* **2003**, *107*, 12569; (c) Neve, F.; LaDeda, M.; Crispini, A.; Bellusci, A.; Puntoriero, F.; Campagna, S. *Organometallics* **2004**, *23*, 5856; (d) Zhao, Q.; Liu, S.; Shi, M.; Wang, C.; Yu, M.; Li, L.; Li, F.; Yi, T.; Huang, C. *Inorg. Chem.* **2006**, *45*, 6152; (e) Kim, K.-Y.; Farley, R. T.; Schanze, K. S. *J. Phys. Chem. B* **2006**, *110*, 17302; (f) Shao, F.; Elias, B.; Lu, W.; Barton, J. K. *Inorg. Chem.* **2007**, *46*, 10187; (g) Yu, M.; Zhao, Q.; Shi, L.; Li, F.; Zhou, Z.; Yang, H.; Yi, T.; Huang, C. *Chem. Commun.* **2008**, 2115; (h) Lincker, F. d. r.; Kreher, D.; Attias, A.-J.; Do, J.; Kim, E.; Hapiot, P.; Lemaître, N. l.; Geffroy, B.; Ulrich, G.; Ziessel, R. *Inorg. Chem.* **2010**, *49*, 3991; (i) Soliman, A. M.; Fortin, D.; Harvey, P. D.; Zysman-Colman, E. *Chem. Commun.* **2012**, *48*, 1120; (j) Kessler, F.; Costa, R. D.; Di Censo, D.; Scopelliti, R.; Ortí, E.; Bolink, H. J.; Meier, S.; Sarfert, W.; Gratzel, M.; Nazeeruddin, M. K.; Baranoff, E. *Dalton Trans.* **2012**, *41*, 180; (k) Hu, T.; Duan, L.; Qiao, J.; He, L.; Zhang, D.; Wang, L.; Qiu, Y. *Synth. Met.* **2013**, *163*, 33; (l) Shavaleev, N. M.; Scopelliti, R.; Grätzel, M.; Nazeeruddin, M. K. *Inorg. Chim. Acta* **2013**, *394*, 295; (m) Constable, E. C.; Housecroft, C. E.; Schneider, G. E.; Zampese, J. A.; Bolink, H. J.; Pertegas, A.; Roldan-Carmona, C. *Dalton Trans.* **2014**, *43*, 4653; (n) Bunzli, A. M.; Bolink, H. J.; Constable, E. C.; Housecroft, C. E.; Junquera-Hernandez, J. M.; Neuburger, M.; Orti, E.; Pertegas, A.; Serrano-Perez, J. J.; Tordera, D.; Zampese, J. A. *Dalton Trans.* **2014**, *43*, 738; (o) Zhang, G.;

Zhang, H.; Gao, Y.; Tao, R.; Xin, L.; Yi, J.; Li, F.; Liu, W.; Qiao, J. *Organometallics* **2013**, *33*, 61.
(8) Donato, L.; McCusker, C. E.; Castellano, F. N.; Zysman-Colman, E. *Inorg. Chem.* **2013**, *52*, 8495.
(9) Soman, S.; Singh Bindra, G.; Paul, A.; Groarke, R.; Manton, J. C.; Connaughton, F. M.; Schulz, M.; Dini, D.; Long, C.; Pryce, M. T.; Vos, J. G. *Dalton Trans.* **2012**, *41*, 12678.
(10) Donato, L.; Abel, P.; Zysman-Colman, E. *Dalton Trans.* **2013**, *42*, 8402.
(11) Pavlishchuk, V. V.; Addison, A. W. *Inorg. Chim. Acta* **2000**, *298*, 97.
(12) For examples see:Ladouceur, S.; Fortin, D.; Zysman-Colman, E. *Inorg. Chem.* **2011**, *50*, 11514
(13) (a) Singh Bindra, G.; Schulz, M.; Paul, A.; Soman, S.; Groarke, R.; Inglis, J.; Pryce, M. T.; Browne, W. R.; Rau, S.; Maclean, B. J.; Vos, J. G. *Dalton Trans.* **2011**, *40*, 10812; (b) Ji, Z.; Huang*, S. D.; Guadalupe*, A. R. *Inorg. Chim. Acta* **2000**, *305*, 127.
(14) Bindra, G. S.; Schulz, M.; Paul, A.; Groarke, R.; Soman, S.; Inglis, J. L.; Browne, W. R.; Pfeffer, M. G.; Rau, S.; MacLean, B. J.; Pryce, M. T.; Vos, J. G. *Dalton Trans* **2012**, *41*, 13050.
(15) D'Alessandro, D. M.; Keene, F. R. *New J. Chem.* **2006**, *30*, 228.
(16) (a) Dixon, I. M.; Collin, J.-P.; Sauvage, J.-P.; Flamigni, L.; Susana, E.; Barigelletti, F. *Chem. Soc. Rev.* **2000**, *29*, 385; (b) Ho, C.-L.; Wong, W. Y.; Zhou, G. J.; Yao, B.; Xie, Z.; Wang, L. *Adv. Funct. Mater.* **2007**, *17*, 2925; (c) Avilov, I.; Minoofar, P.; Cornil, J.; De Cola, L. *J. Am. Chem. Soc.* **2007**, *129*, 8247; (d) Ladouceur, S.; Fortin, D.; Zysman-Colman, E. *Inorg. Chem.* **2010**, *49*, 5625.
(17) (a) Bolink, H. J.; Cappelli, L.; Cheylan, S.; Coronado, E.; Costa, R. D.; Lardies, N.; Nazeeruddin, M. K.; Orti, E. *J. Mater. Chem.* **2007**, *17*, 5032; (b) Costa, R. D.; Monti, F.; Accorsi, G.; Barbieri, A.; Bolink, H. J.; Ortí, E.; Armaroli, N. *Inorg. Chem.* **2011**, *50*, 7229; (c) Ladouceur, S.; Swanick, K. N.; Gallagher-Duval, S.; Ding, Z.; Zysman-Colman, E. *Eur. J. Inorg. Chem.* **2013**, *2013*, 5329.
(18) (a) Zhao, Q.; Yu, M.; Shi, L.; Liu, S.; Li, C.; Shi, M.; Zhou, Z.; Huang, C.; Li, F. *Organometallics* **2010**, *29*, 1085; (b) Langdon-Jones, E. E.; Hallett, A. J.; Routledge, J. D.; Crole, D. A.; Ward, B. D.; Platts, J. A.; Pope, S. J. A. *Inorg. Chem.* **2013**, *52*, 448; (c) Smith, R. A.; Stokes, E. C.; Langdon-Jones, E. E.; Platts, J. A.; Kariuki, B. M.; Hallett, A. J.; Pope, S. J. A. *Dalton Trans.* **2013**, *42*, 10347; (d) Yi, X.; Zhang, C.; Guo, S.; Ma, J.; Zhao, J. *Dalton Trans* **2013**, *43*, 1672; (e) Zhang, G.; Zhang, H.; Gao, Y.; Tao, R.; Xin, L.; Yi, J.; Li, F.; Liu, W.; Qiao, J. *Organometallics* **2013**, **DOI:** 10.1021/om400676h; (f) Constable, E. C.; Housecroft, C. E.; Schneider, G. E.; Zampese, J. A.; Bolink, H. J.; Pertegas, A.; Roldan-Carmona, C. *Dalton Trans* **2014**, *ASAP*, DOI: 10.1039/c3dt53477d.
(19) Ishida, H.; Tobita, S.; Hasegawa, Y.; Katoh, R.; Nozaki, K. *Coord. Chem. Rev.* **2010**, *254*, 2449.
(20) (a) Hohenberg, P.; Kohn, W. *Phys. Rev.* **1964**, *136*, B864; (b) Kohn , W.; Sham, L. J. *Phys. Rev.* **1965**, *140*, A1133; (c) In *The Challenge of d and f Electrons*,; Salahub, D. R., Zerner, M. C., Eds.; ACS: Washington, DC, **1989**; (d) Stratmann, R. E.; Scuseria, G. E.; Frisch, M. J. *J. Chem. Phys.* **1998**, *109*, 8218; (e) Bauernschmitt, R.; Ahlrichs, R. *Chem. Phys. Lett.* **1996**, *256*, 454; (f) Casida, M. E.; Jamorski, C.; Casida, K. C.; Salahub, D. R. *J. Chem. Phys.* **1998**, *108*, 4439.
(21) Frisch, M. J.; Trucks, G. W.; Schlegel, H. B.; Scuseria, G. E.; Robb, M. A.; Cheeseman, J. R.; Zakrzewski, V. G.; Montgomery, J. A.; Stratmann, R. E.; Burant, J. C.; Dapprich, S.; J.M., M.; Daniels, A. D.; Kudin, K. N.; Strain, M. C.; Farkas, O.; Tomasi, J.; Barone, V.; Cossi, M.;

Cammi, R.; Mennucci, B.; Pomelli, C.; Adamo, C.; Clifford, S.; Ochterski, J.; Peterson, G. A.; Ayala, P. Y.; Cui, Q.; Morokuma, K.; Malik, A.; Rabuck, A. D.; Raghavachari, K.; Foresman, J. B.; Cioslowski, J.; Ortiz, J. V.; Baboul, A. G.; Stefanov, B. B.; Liu, G.; Liashenko, A.; Piskorz, P.; Komaromi, I.; Gomperts, R.; Martin, R. L.; Challacombe, M.; Gill, P. M. W.; Johnson, B. G.; Chen, W.; Wong, M. W.; Andres, J. L.; Head-Gordon, M.; Replogle, E. S.; Pople, J. A. *Gaussian 98 (Revision A.6)*; Pittsburgh, PA, **1998**
(22) (a) Becke, A. D. *J. Chem. Phys.* **1993**, *98*, 5648; (b) Lee, C.; Yang, W.; Parr, R. G. *Phys. Rev. B* **1988**, *37*, 785; (c) Miehlich, B.; Savin, A.; Stoll, H.; Preuss, H. *Chem. Phys. Lett.* **1989**, *157*, 200.
(23) (a) Binkley, J. S.; Pople, J. A.; Hehre, W. J. *J. Am. Chem. Soc.* **1980**, *102*, 939; (b) Stevens, W. J.; Basch, W. J.; Krauss, M. *J. Chem. Phys.* **1984**, *81*, 6026; (c) Stevens, W. J.; Krauss, M.; Basch, H.; Jasien, P. G. *Can. J. Chem.* **1992**, *70*, 612; (d) Cundari, T. R.; Stevens, W. J. *J. Chem. Phys.* **1993**, *98*, 5555.
(24) (a) Gordon, M. S.; Binkley, J. S.; Pople, J. A.; Pietro, W. J.; Hehre, W. J. *J. Am. Chem. Soc.* **1982**, *104*, 2797; (b) Pietro, W. J.; Francl, M. M.; Hehre, W. J.; Defrees, D. J.; Pople, J. A.; Binkley, J. S. *J. Am. Chem. Soc.* **1982**, *104*, 5039; (c) Dobbs, K. D.; Hehre, W. J. *J. Comput. Chem.* **1986**, *7*, 359; (d) Dobbs, K. D.; Hehre, W. J. *J. Comput. Chem.* **1987**, *8*, 861; (e) Dobbs, K. D.; Hehre, W. J. *J. Comput. Chem.* **1987**, *8*, 880; (f) Ditchfield, R.; Hehre , W. J.; Pople, J. A. *J. Chem. Phys.* **1971**, *54*, 724; (g) Hehre, W. J.; Ditchfield, R.; Pople, J. A. *J. Chem. Phys.* **1972**, *56*, 2257; (h) Hariharan, P. C.; Pople, J. A. *Theor. Chim. Acta* **1973**, *28*, 213; (i) Hariharan, P. C.; Pople, J. A. *Mol. Phys.* **1974**, *27*, 209; (j) Gordon, M. S. *Chem. Phys. Lett.* **1980**, *76*, 163.
(25) Tomasi, J.; Mennucci, B.; Cammi, R. *Chem. Rev.* **2005**, *105*, 2999.
(26) Baranoff, E.; Bolink, H. J.; Constable, E. C.; Delgado, M.; Haussinger, D.; Housecroft, C. E.; Nazeeruddin, M. K.; Neuburger, M.; Orti, E.; Schneider, G. E.; Tordera, D.; Walliser, R. M.; Zampese, J. A. *Dalton Trans.* **2013**, *42*, 1073.
(27) Nardes, A. M.; Kemerink, M.; de Kok, M. M.; Vinken, E.; Maturova, K.; Janssen, R. A. J. *Org. Electron.* **2008**, *9*, 727.
(28) Nonoyama, M. *Bull. Chem. Soc. Jpn.* **1974**, *47*, 767.
(29) Kozhevnikov, V. N.; Shabunina, O. V.; Kopchuk, D. S.; Ustinova, M. M.; König, B.; Kozhevnikov, D. N. *Tetrahedron* **2008**, *64*, 8963.
(30) (a) Crosby, G. A.; Demas, J. N. *J. Phys. Chem.* **1971**, *75*, 991; (b) Fery-Forgues, S.; Lavabre, D. *J. Chem. Educ.* **1999**, *76*, 1260.

TOC Graphic

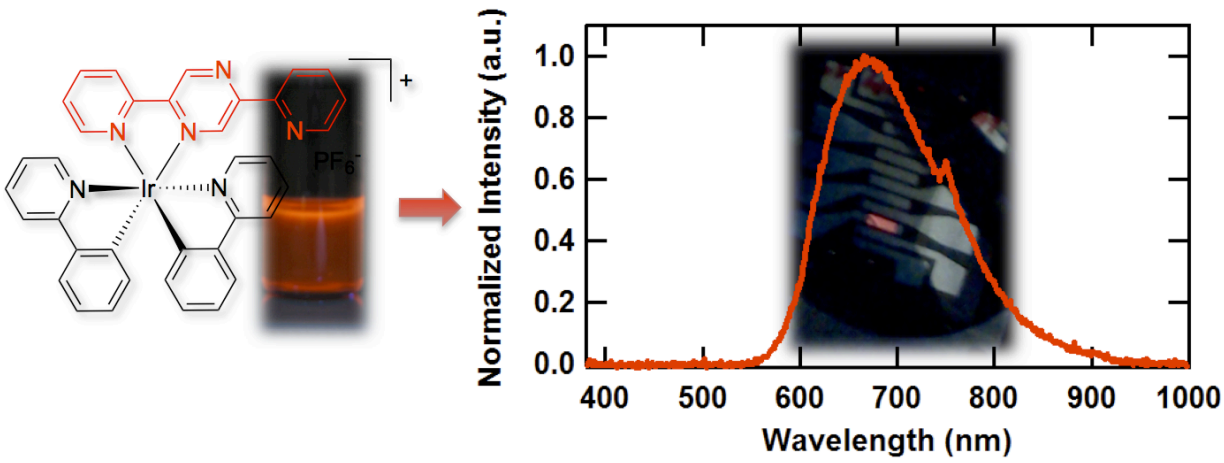
N
N
N
N
Ir
N
+
PF_6^-
Normalized Intensity (a.u.)
0.0
0.2
0.4
0.6
0.8
1.0
400
500
600
700
800
900
1000
Wavelength (nm)